CdTe Quantum Dots as Probes for Near-Infrared Fluorescence Biosensing Using Biocatalytic Growth of Au Nanoparticles

Hongcheng Pan,[†] Rongjing Cui, and Jun-Jie Zhu*

Key Laboratory of Analytical Chemistry for Life Science (MOE), School of Chemistry and Chemical Engineering, Nanjing University, Nanjing 210093, People's Republic of China

Received: August 13, 2008; Revised Manuscript Received: October 3, 2008

A near-infrared (NIR) fluorescence sensing strategy for glucose and xanthine has been developed based on the interaction between CdTe quantum dots (QDs) and biocatalytic generated Au nanoparticles. The fluorescence of CdTe QDs is modulated by changing concentration of $AuCl_4^-$ and Au nanoparticles during the growth process of Au nanoparticles. Two cases were considered. In the first case, the glucose oxidase (GOx) catalyzes the oxidation of glucose to generate H_2O_2. Under the catalysis of Au nanoparticles seeds, the $AuCl_4^-$ is reduced by the H_2O_2 to form the Au nanoparticles. In the second case, the xanthine oxidase acts as the reducing reagents to reduce $AuCl_4^-$ forming Au nanoparticles. The interaction between CdTe quantum dots (QDs), $AuCl_4^-$, and Au nanoparticles resulted in the fluorescence changes of CdTe QDs, allowing the detection of glucose and xanthine. The effects of Au nanoparticles and $AuCl_4^-$ on the fluorescence of CdTe QDs were discussed. A model was developed to explain the mechanism of the CdTe QDs fluorescence changes by biocatalytic growth of Au nanoparticles. The difference in the Stern−Volmer quenching constant between $AuCl_4^-$ and Au nanoparticles is the dominant factor for the CdTe QDs fluorescence changes. The developed method provides low limits of detection, wide linear ranges, and detection wavelengths in the NIR region and can be easily extended to other substrate/oxidase systems.

Introduction

Extensive efforts have been directed toward the development of biosensors based on biocatalytic growth of Au nanoparticles.[1−5] Recently, Willner et al. developed an approach to couple enzymes and metal nanoparticles, using the growth process of metal nanoparticles to identify the substrate, the enzyme activity, or the enzyme inhibition.[6−8] For example, the aptamer-functionalized Au nanoparticles as the catalytic labels were used to develop an optical biosensor for the amplified detection of thrombin.[7] Also, the optical properties of the neurotransmitter-generated Au nanoparticles enable the quantitative analysis of the different neurotransmitters.[8] Using the cholesterol enzyme-modified electrode, an electrochemical approach was applied to detect cholesterol based on the Au nanoparticles growth on the electrode surface.[9] Among these sensing strategies, the optical method is a straightforward approach due to the catalytic generated Au nanoparticles present a plasmon resonance at wavelength of about 540 nm. However, in such visible light region, light is highly absorbed by biological substances, such as hemoglobin, resulting in strong background absorption. A promising alternative for biodetection is to use near-infrared (NIR) light at around 700−1100 nm. The NIR fluorescence is very attractive for biosensing applications because water, hemoglobin, and most biomolecules have their lowest absorption coefficient in the NIR region (700−1100 nm).[10] Moreover, it has the further advantage that there is also less endogenous fluorescence background in the NIR region.[11] CdTe QDs emitting in the NIR regions are of great interest for in vivo biological imaging and diagnostics.[12−16] Recently, the interactions of QDs and Au nanoparticles have attracted increased interest due to their potential applications in sensing technologies.[17,18] Some recent work has shown that the fluorescence of QDs can be enhanced by surface plasmons excited in Au nanoparticles.[19,20] On the other hand, because of the high extinction coefficient and broad absorption spectra, Au nanoparticles were commonly used as a fluorescence quencher and energy acceptor. Accordingly, an inhibition assay of biomolecules was developed based on fluorescence resonance energy transfer between QDs and Au nanoparticles.[21]

Herein, we used CdTe QDs to develop a NIR sensing strategy for oxidase substrates, based on biocatalytic growth of Au nanoparticles. The feasibility of the strategy was demonstrated by detecting two physiologically important substrates, xanthine and glucose. In the case of xanthine, xanthine oxidase was used to reduce Au(III) salts to Au nanoparticles under the catalysis of Au nanoparticles seeds. However, in the case of glucose, the glucose oxidase (GOx) was used as biocatalysts for the in situ generation of H_2O_2 that reduces gold salts. By using CdTe QDs, the approach allows the fluorescence detection in the NIR region. The changes of the fluorescence intensity of CdTe QDs resulted from the changes of the concentrations of $AuCl_4^-$ and Au nanoparticles in the growth process. Both $AuCl_4^-$ and Au nanoparticles have the quenching effects on the fluorescence of CdTe QDs. However, there is a large difference in the quenching constant between $AuCl_4^-$ and Au nanoparticles. Therefore, the fluorescence of CdTe QDs could be significantly changed if the concentrations of $AuCl_4^-$ and Au nanoparticles were slighted changed. The quenching effects of Au nanoparticles and $AuCl_4^-$ on the fluorescence of CdTe QDs were investigated. We demonstrated that the enhancement or quenching of apparent fluorescence depended on the quenching efficiency of $AuCl_4^-$ and generated Au nanoparticles for a fluorophore. The results are useful in the design of fluorescence biosensor by biocatalytic growth of Au nanoparticles.

* Corresponding author: Fax +86-25-83594976; e-mail jjzhu@nju.edu.cn.
[†] Department of Material Science and Chemical Engineering Guilin University of Technology, Guilin 541004, People's Republic of China.

10.1021/jp807251k CCC: $40.75
Published on Web 12/04/2008

SCHEME 1: NIR Fluorescence Strategy for the Detection of (a) Glucose and (b) Xanthine

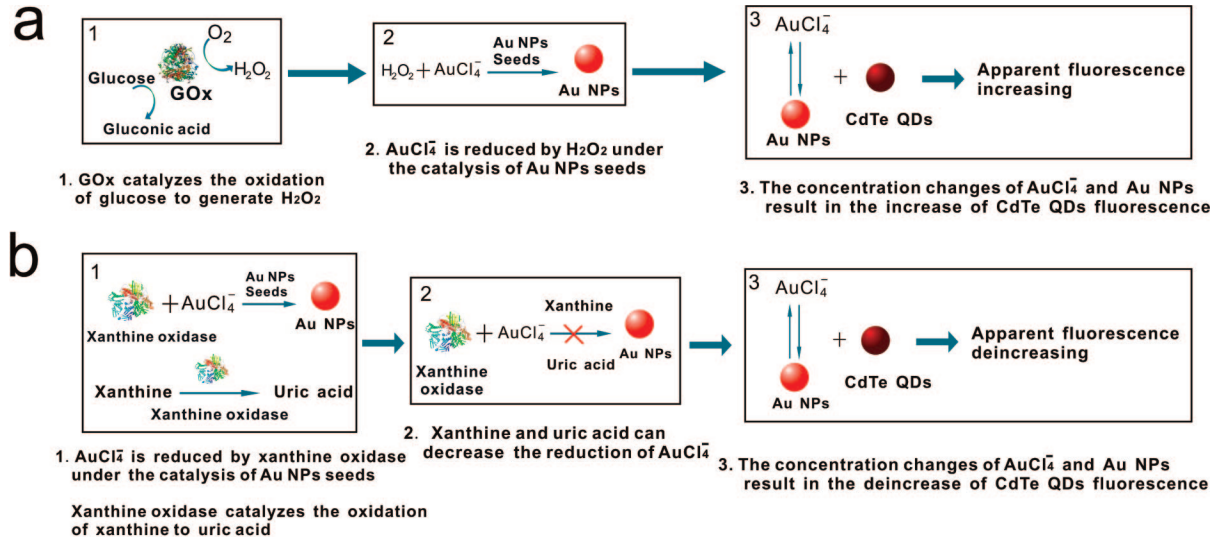

Materials and Methods

Materials. $HAuCl_4 \cdot 4H_2O$ as the precursor for the formation of Au nanoparticles was purchased from Shanghai Sangon Biological Engineering Technology & Services Co. β-Glucose acting as both reducing reagent and capping reagent was supplied by Shanghai Bio Life Science & Technology Co. Sodium hydroxide (NaOH) and sodium citrate were products from Shanghai Chemical Reagent Co. Potssium borohydride (KBH_4) was purchased from Tianjin Chemical Reagent Institute. $CdCl_2 \cdot 2.5H_2O$ was supplied by Shanghai Tingxin Chemical Reagent Factory. Tellurium powder, glucose oxidase, xanthine, xanthine oxidase, and 3-mercaptopropionic acid were purchased from Sigma Chemical Co. Cetyltrimethylammonium chloride (CTAC) was purchased from Shanghai Yongsheng Reagent Factory. Other reagents were of analytical grade. Doubly distilled water was used in all experiments.

Methods. ***Preparation of NIR CdTe QDs.*** CdTe QDs were synthesized according to the modifications of the literature procedure.[13,22,23] Briefly, 198 mL of doubly distilled water was degassed by bubbling nitrogen for 1 h. 0.1142 g of 0.5 mmol $CdCl_2 \cdot 2.5H_2O$ and 0.0849 g of 0.8 mmol 3-mercaptopropionic acid (MPA) were added into the solution, and the pH was adjusted to 8.0−8.5 by the addition of 5% NaOH solution. The mixing solution was refluxed and bubbled with nitrogen for 30 min. Subsequently, 2 mL of freshly prepared KHTe solution was mixed with the above CdCl−MPA solution. The KHTe solution was produced by the reaction of 0.0480 g of 0.89 mmmol KBH_4 with 0.0480 g of 0.375 mmol tellurium powder in a 2 mL aqueous solution. The resulting mixture solution was refluxed under nitrogen flow at 96−99 °C for different times to obtain the CdTe QDs with different sizes. CdTe QDs with tunable emission in the visible and NIR region (up to about 750 nm) were synthesized. The size and emission wavelength of the CdTe QDs was controlled by the duration of reflux. The samples were stored in darkness for 24 h before the fluorescence spectra were taken.

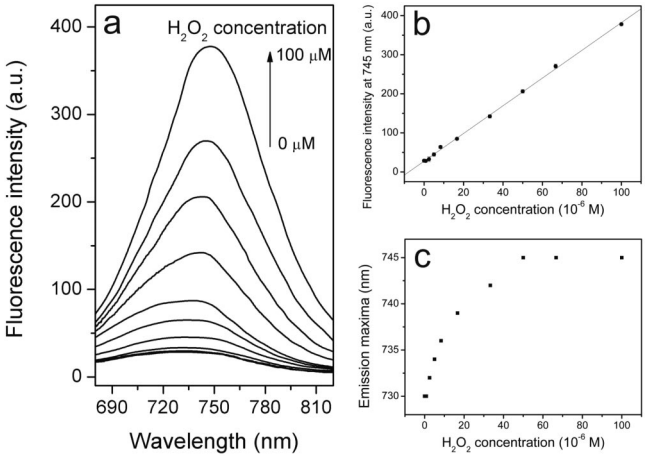

Figure 1. (a) Variation in the fluorescence spectra of CdTe QDs solution (1 mL, 1.8 mM) mixing with 5 mL of the Au nanoparticles growth solution (containing 1.8×10^{-6} M Au seeds, 2.4×10^{-4} M $HAuCl_4$, 2.0×10^{-3} M CTAC, 0.01 M PBS pH 7.05, reacting with different concentrations of H_2O_2). (b) Fluorescence intensity at 745 nm vs H_2O_2 concentration. (c) Emission maxima vs H_2O_2 concentration.

Preparation of Au Nanoparticle Seeds. Au nanoparticle seeds were prepared by using KBH_4 as a reductant and stabilized with sodium citrate following the literature.[24,25] 5 mL of 1% $HAuCl_4$ and 10 mL of 0.03 M sodium citrate were added into 250 mL of doubly distilled water and stirred. Then 5 mL of freshly prepared 0.1 M KBH_4 was added, and the mixture solution was allowed to stir at room temperature for 24 h. The diameter of the Au nanoparticle seeds was about 4−7 nm.

Growth of Au Nanoparticles and NIR Fluorescence Sensing for H_2O_2, β-Glucose, and Xanthine. The Au nanoparticles growth solution consisted of 2.4×10^{-4} M $HAuCl_4$ and 2.0×10^{-3} M CTAC in 0.01 M phosphate-buffered saline (PBS), pH 7.05. For the detection of H_2O_2, β-glucose, and xanthine, different concentrations of H_2O_2 and β-glucose together with 47 μg/mL GOx or xanthine together with 1 U xanthine oxidase were added to 5 mL of the growth solution, respectively. Then 20 μL of 4.5×10^{-4} M Au nanoparticle seeds was added to the growth solution for the catalytic growth of the Au nanoparticles. The growth processes were performed at room temperature of 5 °C for 5 h in the case of H_2O_2, 37 °C for 3 h in the case of β-glucose, or 37 °C for 8 h in the case of xanthine. Subsequently, 1 mL of 1.8 mM NIR CdTe QDs was added to the solution. After 20 min at 25 °C, the fluorescence spectra were recorded with an excitation wavelength of 420 nm. Absorption and fluorescence spectra were recorded on a Shimadzu UV-3600 UV−vis−NIR spectrophotometer and a Hitachi 850 fluorescence spectrophotometer, respectively.

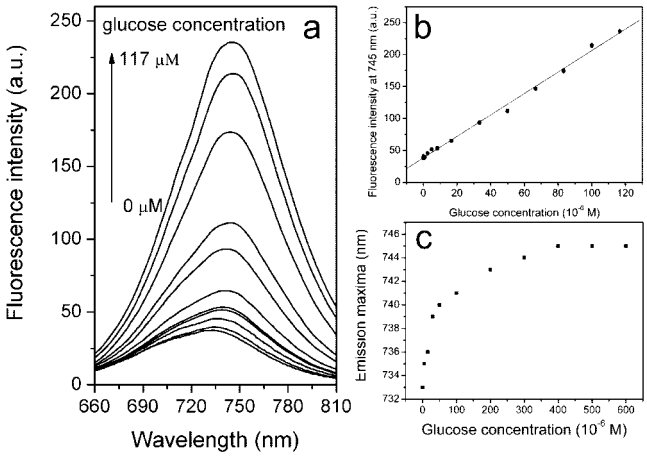

Figure 2. (a) Variation in the fluorescence spectra of CdTe QDs solution (1 mL, 1.8 mM) mixing with 5 mL of the Au nanoparticles growth solution (containing 1.8×10^{-6} M Au seeds, 2.4×10^{-4} M $HAuCl_4$, 2.0×10^{-3} M CTAC, 47 μg/mL GOx, 0.01 M PBS pH 7.05, reacting with different concentrations of glucose). (b) Fluorescence intensity at 745 nm vs glucose concentration. (c) Emission maxima vs glucose concentration.

Results and Discussion

The NIR fluorescence strategy for the detection of glucose and xanthine is illustrated in Scheme 1. In the experiments, Au nanoparticles can be generated in the growth solution by two approaches: H_2O_2 or xanthine oxidase acted as reducing reagents. In the first case, the glucose oxidase catalyzes the oxidation of glucose to generate H_2O_2. And the $AuCl_4^-$ is reduced by the H_2O_2 under the catalysis of Au nanoparticles seeds.[26] In the second case, xanthine oxidase acted as the reducing reagents can generate Au nanoparticles. We used the generated Au nanoparticles to interact with CdTe QDs for developing a NIR fluorescence-sensing strategy for glucose and xanthine.

NIR Fluorescence Sensing for Glucose. Figures 1 and 2 show the NIR fluorescence sensing for glucose by using CdTe QDs. The glucose oxidase catalyzes the oxidation of glucose to gluconic acid and H_2O_2. The latter product can be used to reduce $AuCl_4^-$ to Au nanoparticles. Since the amount of the formed H_2O_2 is controlled by the concentration of glucose, the concentration of generated Au nanoparticles is dominated by the concentration of glucose. After the generation of Au nanoparticles, 1 mL of 1.8 mM CdTe QDs solution with emission maximum at 740 nm was added into the growth solution. The maximum emission of CdTe QDs shifted to 730 nm in the growth solution. However, when the CdTe QDs solution was added into the growth solution with the different Au nanoparticles concentration, a pronounced enhancement of QDs emission was observed with the increase of Au nanoparticle concentration, as shown in Figures 1a and 2a. As reported in the literature, the fluorescence of QDs can be quenched by H_2O_2.[27] However, the effect of H_2O_2 on QDs emission could be negligible in the experiments because the H_2O_2 was consumed completely in the presence of excess $AuCl_4^-$. Therefore, as shown in Figures 1c and 2c, with the fluorescence intensity growth, a red shift in the emission maxima occurs from 730 to 745 nm in the case of H_2O_2 and from 735 to 745 nm in the case of glucose. Figures 1b and 2b show the calibration curve derived from the changes in the fluorescence at $\lambda = 745$ nm as the concentration of H_2O_2 and glucose increases, respectively. The limit of detection for H_2O_2 and glucose is 2.4×10^{-6} and 2.7×10^{-6} M, respectively. The linear concentration ranges for H_2O_2 and glucose are from 5.0×10^{-6} to 1.0×10^{-4} M and from 5.0×10^{-6} to 1.2×10^{-4} M, respectively. More importantly, by using this strategy, one could detect glucose at wavelength in the NIR region instead of the visible light region.

Mechanism of the Fluorescence Changes. The effects of Au nanoparticles and $AuCl_4^-$ on the CdTe fluorescence were also investigated. The Au nanoparticles with a diameter of 7 nm were selected to study the effect of the Au nanoparticles on the CdTe QDs fluorescence. Figure 3 shows the fluorescence intensities of CdTe QDs in the presence of Au nanoparticles. With the Au nanoparticles concentration increased, the emission intensity decreased gradually, and no significant shifts were observed in the emission maximum. The possible quenching mechanism can be studied by determining quenching rate parameters using Stern−Volmer (S−V) plots that are drawn in accordance with the S−V equation:[28,29]

$$\frac{F_0}{F} = 1 + K_{SV}[Q] \quad (1)$$

where F_0 and F denote the steady-state fluorescence intensities in the absence and in the presence of quencher, respectively, K_{SV} is the Stern−Volmer quenching constant, and [Q] is the concentration of quencher. The different mechanisms of quenching are usually classified as either dynamic quenching or static quenching. Dynamic and static quenching can be distinguished by their differing dependence on temperature and excited-state lifetime. Dynamic quenching depends upon diffusion. Since higher temperatures result in faster diffusion, hence quenching constants are expected to increase with increasing temperature.

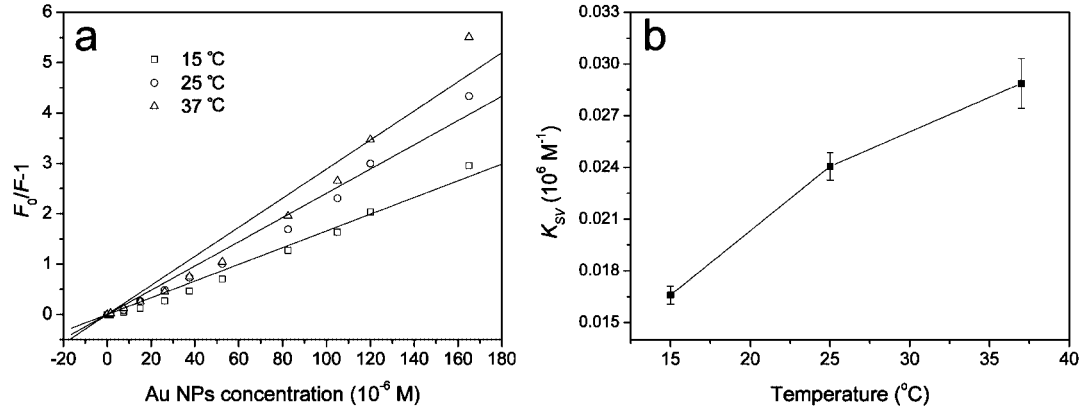

Figure 3. (a) S−V plots of the fluorescence quenching of CdTe QDs by Au nanoparticles at 15, 25, and 37 °C. (b) K_{sv} vs temperature.

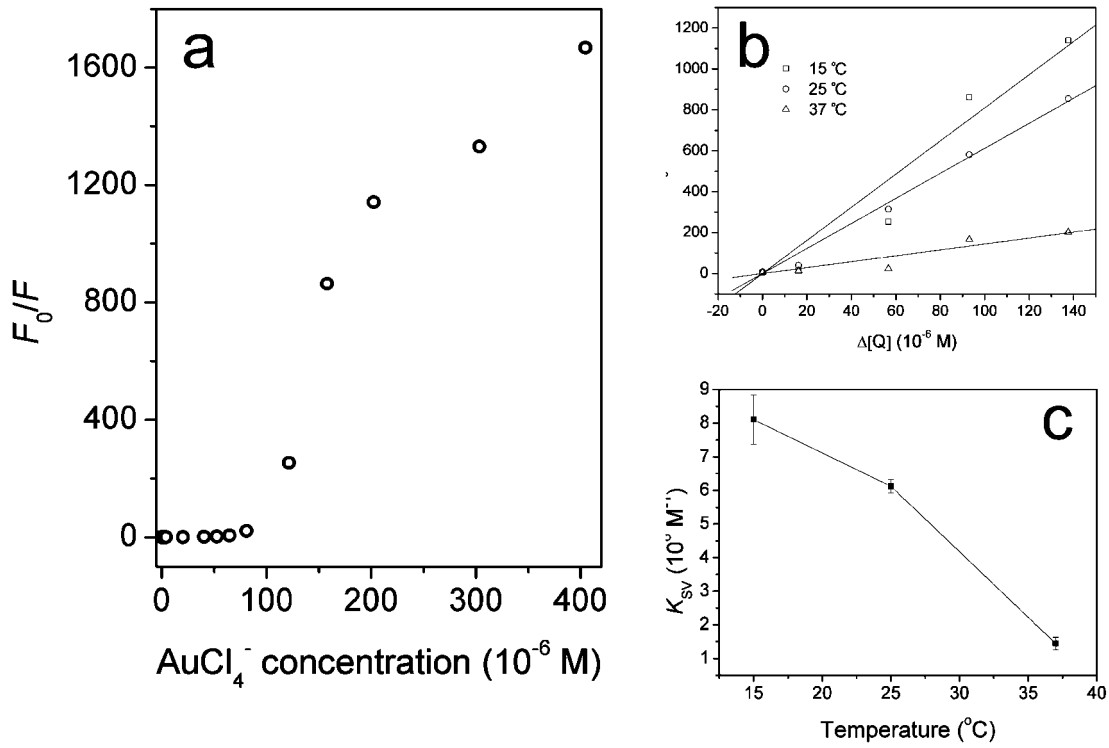

Figure 4. (a) S−V plots of the fluorescence quenching of CdTe QDs by $AuCl_4^-$ at 25 °C. (b) S−V plots of $F_0/F - 1$ vs Δ[Q] at 15, 25, and 37 °C. (c) K_{SV} vs temperature.

In contrast, increased temperature is likely to result in the dissociation of weakly bound complexes and thus lower values of the static quenching constants. Figure 3a shows the S−V plots of the fluorescence quenching of CdTe QDs by Au nanoparticles at different temperatures. The corresponding Stern−Volmer quenching constants at different temperatures are shown in Figure 3b. The linearity of the S−V plots is indicative of a single quenching mechanism either static or dynamic. On the contrary, the characteristic S−V plot of combined quenching both static and dynamic is an upward curvature. The values of K_{SV} increase as the temperature increases, indicating that the quenching mechanism is mainly a dynamic process resulting from diffusive encounters between QDs and Au nanoparticles during the lifetime of excited state.

In the case of $AuCl_4^-$, the quenching mechanism is more complicated than that of Au nanoparticles. Figure 4 shows the fluorescence intensities of CdTe QDs in the presence of $AuCl_4^-$. As the concentration of $AuCl_4^-$ increases, the fluorescence intensity of CdTe QDs increases and the emission maximum shifted from 745 to 732 nm. The corresponding S−V plot of the emission intensity in Figure 4a shows strong upward curvature at higher $AuCl_4^-$ concentrations. Such behavior is diagnostic of an additional deactivation pathway involving static quenching.[30] Further quenching experiments were carried out at three different temperatures of 15, 25, and 37 °C. The S−V plots were not linear over the investigated concentration range. However, as shown in Figure 4b, the S−V plot is approximately linear in the concentrations from 6.47×10^{-5} to 2.02×10^{-4} M, implying that dynamic or static quenching is the dominant mechanism at higher concentrations. In the Au nanoparticles growth process, the $AuCl_4^-$ concentration typically decreased from 2.02×10^{-4} to 1.35×10^{-4} M, corresponding to H_2O_2 concentration range from 0 to 1×10^{-4} M. The dependence of K_{SV} on $AuCl_4^-$ concentration ([Q]) ranging from 6.40×10^{-5} to 2.02×10^{-4} M was obtained. We define a parameter, $\Delta[Q] = [Q] - [Q]'$ ([Q]′ is initial concentration of the linear concentration range; here we set $[Q]' = 6.47 \times 10^{-5}$ M), to represent net increase of $AuCl_4^-$ in the concentration range. The S−V plots of $F_0/F - 1$ against Δ[Q] at different temperatures are shown in Figure 4b. Figure 4c shows that the K_{SV} values decrease with temperature increases. The decreasing trend of K_{SV} can be attributed to the nonfluorescent ground-state complex would possibly be partly decomposed when the temperature increases.

A model is proposed to explain the mechanism by using H_2O_2 as a model reducing reagent. Assuming that the fluorescence changes of CdTe QDs are due to two quenchers present in concentrations $[Q]_a$ for $AuCl_4^-$ and $[Q]_b$for generated Au nanoparticles, their contribution to the overall quenching process is given by

$$\frac{d\left(\frac{F_c}{F}\right)}{d[H_2O_2]} = \frac{d\left(\frac{F_0}{F_a}\right)}{d[Q]_a} + \frac{d\left(\frac{F_0}{F_b}\right)}{d[Q]_b} \quad (2)$$

where F_c is the fluorescence intensity of CdTe QDs in the presence of the Au nanoparticles growth solution. F is the fluorescence intensity of CdTe QDs in the presence of the Au nanoparticles growth solution after the addition of H_2O_2. F_0 is the fluorescence intensity of CdTe QDs in the presence of a blank solution (containing 2.0×10^{-3} M CTAC, 0.01 M PBS pH 7.05). F_a is the fluorescence intensity of CdTe QDs in the presence of the blank solution with $AuCl_4^-$. F_b is the fluorescence intensity of CdTe QDs in the presence of the blank solution with Au nanoparticles. $[H_2O_2]$, $[Q]_a$, and $[Q]_b$ are the concentration of H_2O_2, $AuCl_4^-$, and Au nanoparticles, respectively. According to the reaction equation

$$AuCl_4^- + 3/2H_2O_2 \xrightarrow{\text{Au NP seeds}} Au^0 + 4HCl + 3/2O_2 \quad (3)$$

$[Q]_a = [Q]_0 - [Q]_b$, $\Delta[Q] = [Q]_0 - [Q]_a$, and $[Q]_b = 1.5[Q]_c$ are obtained, where $[Q]_0 = 2.4 \times 10^{-4}$ M. In the case of $AuCl_4^-$ or Au nanoparticles as single quencher, the corresponding S−V equation can be written as

$$\frac{d\left(\frac{F_0}{F_a}\right)}{d(\Delta[Q])} = {}^aK_{SV} \quad (4)$$

$$\frac{d\left(\frac{F_0}{F_b}\right)}{d([Q]_b)} = {}^bK_{SV} \quad (5)$$

where ${}^aK_{SV}$ and ${}^bK_{SV}$ are the Stern−Volmer quenching constant of $AuCl_4^-$ and Au nanoparticles, respectively. Substituting $\Delta[Q] = [Q]_0 - [Q]_a$ into eq 4, we can obtain

$$\frac{d\left(\frac{F_0}{F_a}\right)}{d(\Delta[Q])} = \frac{d\left(\frac{F_0}{F_a}\right)}{d([Q]_0 - [Q]_a)} = -\frac{d\left(\frac{F_0}{F_a}\right)}{d([Q]_a)} = -{}^aK_{SV} \quad (6)$$

then we get the overall quenching equation from eqs 2, 5, and 6 as

$$\frac{d\left(\frac{F_c}{F}\right)}{d[H_2O_2]} = {}^bK_{SV} - {}^aK_{SV} \quad (7)$$

Equation 7 shows that the rate of change of total fluorescence intensity depends on the value of $({}^bK_{SV} - {}^aK_{SV})$. From the S−V plot in Figures 5b and 6c, the values of ${}^aK_{SV}$ and ${}^bK_{SV}$ are obtained. In this present work, we get ${}^bK_{SV} - {}^aK_{SV} < 0$ at three temperatures. Mathematically, if $d(F_c/F)/d[H_2O_2] < 0$, the value of F_c/F decreases with the increasing of $[H_2O_2]$. In other words, the CdTe QDs fluorescence increases with the increase of H_2O_2 or glucose. Equation 7 is in good agreement with the experimental data. On the basis of the model, we address the mechanism of apparent fluorescence enhancement of CdTe QDs by biocatalytic growth of Au nanoparticles. The key reason is that the Stern−Volmer quenching constant of $AuCl_4^-$ is larger than that of Au nanoparticles. During the growth process of Au nanoparticles, $AuCl_4^-$ is reduced to form Au nanoparticles, which leads to a suppression in fluorescence quenching of CdTe QDs by $AuCl_4^-$.

NIR Fluorescence Sensing for Xanthine. Figure 5 shows that CdTe QDs were applied to detect xanthine. The results were very different from those in the case of glucose. The fluorescence of CdTe QDs was quenched by adding to the growth solutions with increased concentrations of xanthine (Figure 5a,b). Concomitant to the fluorescence intensity quenching, a blue shift in the emission maxima occurs from 741 to 729 nm (Figure 5c).

We found that xanthine oxidase could reduce $AuCl_4^-$ to Au nanoparticles. Figure 6a shows that as the concentration of xanthine oxidase increases in the absence of xanthine, the absorbance plasmon of the generated Au nanoparticles is intensified. In the presence of xanthine, the xanthine oxidase catalyzes the oxidation of xanthine to uric acid. However, the

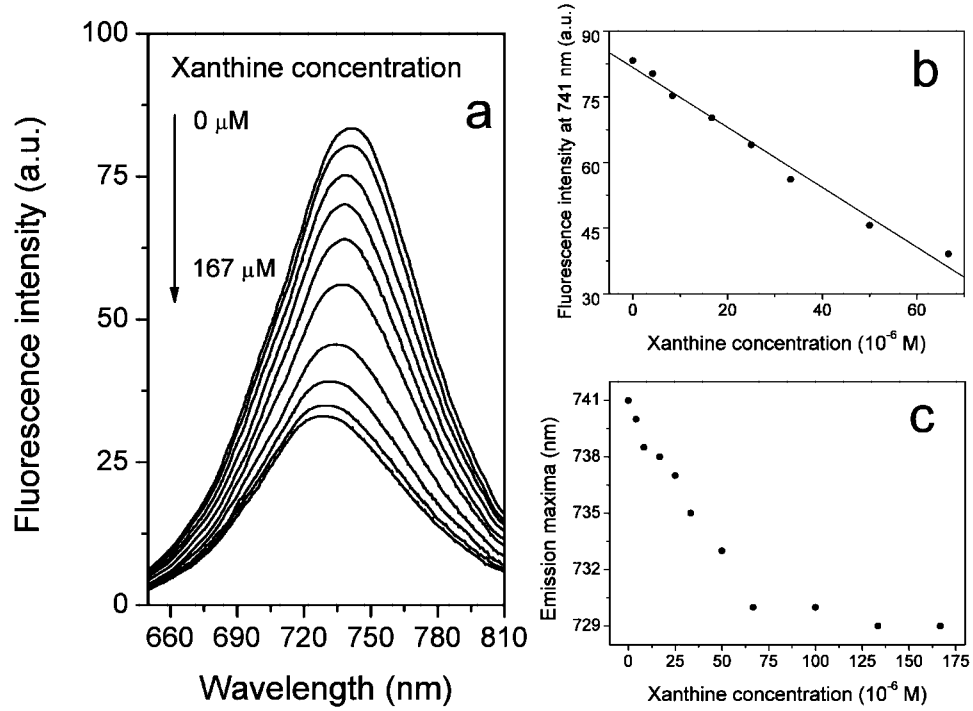

Figure 5. (a) Variation in the fluorescence spectra of CdTe QDs solution (1 mL, 1.8 mM) mixing with 5 mL of the Au nanoparticles growth solution (containing 4.5×10^{-5} M Au seeds, 2.4×10^{-4} M $HAuCl_4$, 2.0×10^{-3} M CTAC, 1 U xanthine oxidase, 0.01 M PBS pH 7.05, reacting with different concentrations of xanthine). (b) Fluorescence intensity at 741 nm vs xanthine concentration. (c) Emission maxima vs xanthine concentration.

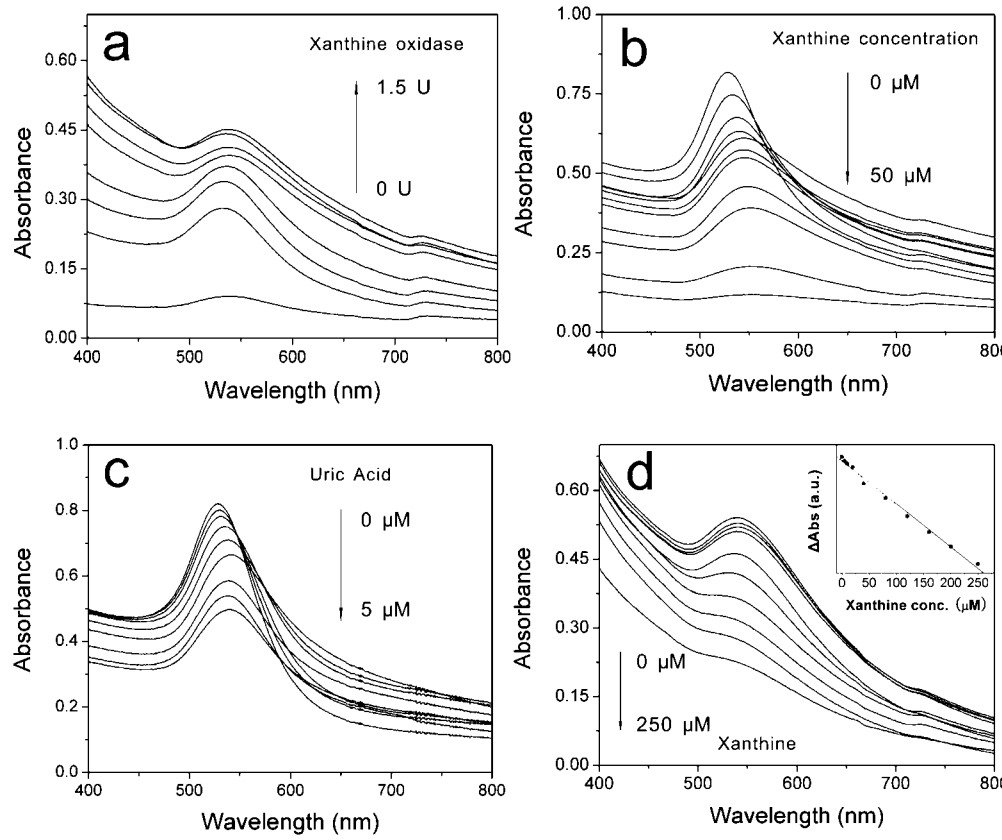

Figure 6. Variation in the absorbance spectra of the Au nanoparticles growth solution (containing 4.5×10^{-5} M Au seeds, 2.4×10^{-4} M $HAuCl_4$, 2.0×10^{-3} M CTAC, 0.01 M PBS pH 7.05): (a) at different concentrations of xanthine oxidase; (b) at 3×10^{-4} M H_2O_2 and different concentrations of xanthine; (c) at 3×10^{-4} M H_2O_2 and different concentrations of uric acid; (d) at 1 U xanthine oxidase and different concentrations of xanthine. Inset: relative absorbance (ΔAbs) at 532 nm vs xanthine concentration.

presence of xanthine and uric acid was found to decrease the reduction of $AuCl_4^-$. To separately study the effect of xanthine and uric acid on the reduction of $AuCl_4^-$, we used H_2O_2 as a model reducing reagent to reduce $AuCl_4^-$. The results in Figure 6b,c indicate that the generated Au nanoparticles decrease with the increase of the xanthine and uric acid, reflecting in the increase of plasmon absorbance of Au nanoparticles. Therefore, the concentration of generated Au nanoparticles in the growth solution can be written as follows

$$[\text{Au NPs}] = k_1[\text{XO}]_0 - k_2[\text{X}] - k_3[\text{UA}] \qquad (8)$$

where [Au NPs] is the concentration of generated Au nanoparticles. $[XO]_0$ is the initial concentration of xanthine oxidase. [X] and [UA] are the concentration of free xanthine and uric acid, respectively. k_1, k_2, and k_3 are the influence coefficient of xanthine oxidase, xanthine, and uric acid on the reduction of $AuCl_4^-$, respectively. According to the oxidation reaction of xanthine

$$\text{xanthine} \xrightarrow{\text{xanthine oxidase}} \text{uric acid} \qquad (9)$$

the concentration of uric acid can be written as

$$[\text{UA}] = \frac{\alpha}{1-\alpha}[\text{X}] \qquad (10)$$

where α is the conversion ratio of xanthine to uric acid. Substituting eq 10 into eq 8, we can obtain

$$[\text{Au NPs}] = K - \left(k_2 + \frac{\alpha k_3}{1-\alpha}\right)[\text{X}] \qquad (11)$$

where $K = k_1[XO]_0$. Equation 11 reversals that the concentration of generated Au nanoparticles decreases with increasing xanthine, which is in agreement with the experimental results shown in the inset of Figure 6d. In the experiments, in order to subtract background signals, we substitute the relative absorbance (ΔAbs) for the absolute absorbance (Abs). We defined relative absorbance as $\Delta\text{Abs} = \text{Abs} - \text{Abs}_0$, where Abs is the absolute absorbance at 532 nm of the Au nanoparticles growth solution (containing 4.5×10^{-5} M Au seeds, 2.4×10^{-4} M $HAuCl_4$, 2.0×10^{-3} M CTAC, 0.01 M PBS pH 7.05) at 1 U xanthine oxidase and different concentrations of xanthine, Abs_0 is the absolute absorbance at 532 nm of the Au nanoparticles growth solution at 1 U xanthine oxidase and xanthine concentrations of 250 μM. The inset of Figure 6d shows that there is a linear dependence of the relative absorbance (ΔAbs) of generated Au nanoparticles at 532 nm on xanthine concentration in the range of 5×10^{-6}–2.5×10^{-4} M.

Further fluorescence detection is based on the interactions between $AuCl_4^-$, the generated Au nanoparticles, and CdTe QDs. Figure 5b shows the calibration curve derived from the quenching in the fluorescence intensity at $\lambda = 741$ nm as the concentration of xanthine increases. The linear concentration range is from 4.2×10^{-6} to 6.7×10^{-5} M, and the limit of

detection is 1.8×10^{-6} M. Assuming that the generated Au nanoparticles and $AuCl_4^-$ are dominant influences on the quenching of CdTe QDs, the overall fluorescence equation (2) in the case of xanthine oxidase can be expressed as

$$\frac{d\left(\frac{F_x}{F_1}\right)}{d[X]} = \frac{d\left(\frac{F_0}{F_a}\right)}{d[Q]_a} + \frac{d\left(\frac{F_0}{F_a}\right)}{d[Q]_b} \quad (12)$$

where F_x is the fluorescence intensity of CdTe QDs in the presence of the Au nanoparticles growth solution. F_1 is the fluorescence intensity of CdTe QDs in the presence of the Au nanoparticles growth solution after the addition of xanthine/xanthine oxidase. In the case of xanthine oxidase, eq 11 shows the concentration of generated Au nanoparticles decreases with the increasing of xanthine. Therefore, eq 12 can be rewritten as

$$\frac{d\left(\frac{F_x}{F_1}\right)}{d[X]} = \frac{d\left(\frac{F_0}{F_a}\right)}{d[Q]_a} + \frac{d\left(\frac{F_0}{F_b}\right)}{d[Q]_b} = {}^aK_{SV} - {}^bK_{SV} \quad (13)$$

As discussed above, we get ${}^aK_{SV} - {}^bK_{SV} > 0$. The result indicates the intensity of CdTe QDs fluorescence decreases with the increase of xanthine and is in agreement with the experiment.

Conclusion

A highly sensitive NIR fluorescence sensing strategy for glucose and xanthine has been developed based on the fluorescence changes of CdTe QDs with the biocatalytic growth of the Au nanoparticles. Different from the previously reported method that utilizes plasma absorption of Au nanoparticles as sensing signal, the fluorescence strategy can achieve a lower limit of detection. Importantly, the method offers a detection wavelength at the NIR region, which could avoid interference from absorption and autofluorescence of most biological substances. We investigated the quenching effects of Au nanoparticles and $AuCl_4^-$ on the fluorescence of CdTe QDs. Accordingly, we developed a model to describe the mechanism of the fluorescence changes of CdTe QDs. The results demonstrated that the difference of Stern−Volmer quenching constant between $AuCl_4^-$ and generated Au nanoparticles plays the most important role in the change of fluorescence intensity. We consider two cases, one in which glucose/glucose oxidase-generated H_2O_2 acts as reducing reagent and another in which xanthine oxidase could reduce $AuCl_4^-$. In the first case, if the Stern−Volmer quenching constant of $AuCl_4^-$ for a fluorophore is larger than that of Au nanoparticles, namely ${}^bK_{SV} - {}^aK_{SV} < 0$, the apparent fluorescence of a fluorophorer would be increased with the increase of reducer concentration after a growth process of Au nanoparticles. However, in the second case, if ${}^bK_{SV} - {}^aK_{SV} < 0$, the apparent fluorescence would be decreased with the increase of the xanthine concentration. The results are in good agreement with the experimental data.

Acknowledgment. We greatly appreciate the support of the National Natural Science Foundation of China (Nos. 20635020, 90606016, 20521503) and Natural Science Foundation of Guangxi, China. This work is also supported by National Basic Research Program of China (2006CB933201).

References and Notes

(1) Zayats, M.; Baron, R.; Popov, I.; Willner, I. *Nano Lett.* **2005**, *5*, 21.
(2) Park, S. J.; Taton, T. A.; Mirkin, C. A. *Science* **2002**, *295*, 1503.
(3) Willner, I.; Patolsky, F.; Weizmann, Y.; Willner, B. *Talanta* **2002**, *56*, 847.
(4) Weizmann, Y.; Patolsky, F.; Willner, I. *Analyst* **2001**, *126*, 1502.
(5) Willner, I.; Baron, R.; Willner, B. *Adv. Mater.* **2006**, *18*, 1109.
(6) Xiao, Y.; Pavlov, V.; Levine, S.; Niazov, T.; Markovitch, G.; Willner, I. *Angew. Chem., Int. Ed.* **2004**, *43*, 4519.
(7) Pavlov, V.; Xiao, Y.; Shlyahovsky, B.; Willner, I. *J. Am. Chem. Soc.* **2004**, *126*, 11768.
(8) Baron, R.; Zayats, M.; Willner, I. *Anal. Chem.* **2005**, *77*, 1566.
(9) Zhou, N.; Wang, J.; Chen, T.; Yu, Z.; Li, G. *Anal. Chem.* **2006**, *78*, 5227.
(10) Pham, W.; Lai, W. F.; Weissleder, R.; Tung, C. H. *Bioconjugate Chem.* **2003**, *14*, 1048.
(11) Kiyose, K.; Kojima, H.; Urano, Y.; Nagano, T. *J. Am. Chem. Soc.* **2006**, *128*, 6548.
(12) Li, L.; Qian, H.; Ren, J. *Chem. Commun.* **2005**, *4*, 528.
(13) Gaponik, N.; Talapin, D. V.; Rogach, A. L.; Hoppe, K.; Shevchenko, E. V.; Kornowski, A.; Eychmüller, A.; Weller, H. *J. Phys. Chem. B* **2002**, *106*, 7177.
(14) Gaponik, N.; Radtchenko, I. L.; Sukhorukov, G. B.; Weller, H.; Rogach, A. L. *Adv. Mater.* **2002**, *14*, 879.
(15) Li, J. J.; Tsay, J. M.; Michalet, X.; Weiss, S. *Chem. Phys.* **2005**, *318*, 82.
(16) Qian, H.; Dong, C.; Peng, J.; Qiu, X.; Xu, Y.; Ren, J. *J. Phys. Chem. C* **2007**, *111*, 16852.
(17) Nikoobakht, B.; Burda, C.; Braun, M.; Hun, M.; El-Sayed, M. A. *Photochem. Photobiol.* **2002**, *75*, 591.
(18) Liu, N.; Prall, B. S.; Klimov, V. I. *J. Am. Chem. Soc.* **2006**, *128*, 15362.
(19) Kulakovich, O.; Strekal, N.; Yaroshevich, A.; Maskevich, S.; Gaponenko, S.; Nabiev, I.; Woggon, U.; Artemyev, M. *Nano Lett.* **2002**, *2*, 1449.
(20) Fu, A.; Micheel, C. M.; Cha, J.; Chang, H.; Yang, H.; Alivisatos, A. P. *J. Am. Chem. Soc.* **2004**, *126*, 10832.
(21) Oh, E.; Hong, M. Y.; Lee, D.; Nam, S. H.; Yoon, H. C.; Kim, H. S. *J. Am. Chem. Soc.* **2005**, *127*, 3270.
(22) Zhang, H.; Wang, D.; Yang, B.; Mohwald, H. *J. Am. Chem. Soc.* **2006**, *128*, 10171.
(23) Weng, J.; Song, X.; Li, L.; Qian, H.; Chen, K.; Xu, X.; Cao, C.; Ren, J. *Talanta* **2006**, *70*, 397.
(24) Zhou, N.; Wang, J.; Chen, T.; Yu, Z.; Li, G. *Anal. Chem.* **2006**, *78*, 5227.
(25) Busbee, B. D.; Obare, S. O.; Murphy, C. J. *Adv. Mater.* **2003**, *15*, 414.
(26) Zayats, M.; Baron, R.; Popov, I.; Willner, I. *Nano Lett.* **2005**, *5*, 21.
(27) Gill, R.; Bahshi, L.; Freeman, R.; Willner, I. *Angew. Chem., Int. Ed.* **2008**, *47*, 1676.
(28) Yuan, P.; Walt, D. R. *Anal. Chem.* **1987**, *59*, 2391.
(29) Geddes, C. D. *Meas. Sci. Technol.* **2001**, *12*, R53.
(30) Watson, R. T.; Desai, N.; Wildsmith, J.; Wheeler, J. F.; Kane-Maguire, N. A. P. *Inorg. Chem.* **1999**, *38*, 2683.

JP807251K